Hard-core boson approach to the spin-$\frac{1}{2}$ triangular-lattice antiferromagnet Cs_2CuCl_4 at finite temperatures in magnetic fields higher than the saturation field

Simon Streib* and Peter Kopietz

Institut für Theoretische Physik, Universität Frankfurt, Max-von-Laue Strasse 1, 60438 Frankfurt, Germany

(Received 23 July 2015; published 30 September 2015)

We study the high magnetic field regime of the antiferromagnetic insulator Cs_2CuCl_4 by expressing the spin-1/2 operators in the relevant Heisenberg model in terms of hard-core bosons and implementing the hard-core constraint via an infinite on-site interaction. We focus on the case where the external magnetic field exceeds the saturation field $B_c \approx 8.5$ T and is oriented along the crystallographic a axis perpendicular to the lattice plane. Because in this case the excited states are separated by an energy gap from the ground state, we may use the self-consistent ladder approximation to take the strong correlations due to the hard-core constraint into account. In Cs_2CuCl_4, there are additional interactions besides the hard-core interaction which we treat in self-consistent Hartree-Fock approximation. We calculate the spectral function of the hard-core bosons from which we obtain the in-plane components of the dynamic structure factor, the magnetic susceptibility, and the specific heat. Our results for the specific heat are in good agreement with the available experimental data. We conclude that the self-consistent ladder approximation in combination with a self-consistent Hartree-Fock decoupling of the non-hard-core interactions gives an accurate description of the physical properties of gapped hard-core bosons in two dimensions at finite temperatures.

DOI: 10.1103/PhysRevB.92.094442 PACS number(s): 75.10.Jm, 05.30.Jp, 75.40.Cx, 75.40.Gb

I. INTRODUCTION

The magnetic behavior of the antiferromagnetic insulator Cs_2CuCl_4 can be described by a spin-1/2 Heisenberg model on a triangular lattice where the interlayer coupling is much weaker than the intralayer couplings. Due to the relatively weak exchange couplings, a field-induced ferromagnetic ground-state can be reached at fields larger than the saturation field $B_c \approx 8.5$ T where the magnetic field is along the crystallographic a axis perpendicular to the lattice plane. This allows a precise measurement of the exchange couplings via inelastic neutron scattering experiments where the single magnon dispersion gives direct access to the exchange couplings [1]. Cs_2CuCl_4 has been intensively studied due to its interesting properties, e.g., spin-liquid behavior with spinon excitations [2–14], Bose-Einstein condensation of magnons at the quantum critical point [1,15–18], and a rich phase diagram for in-plane magnetic fields [2,19–24]. A diverse range of observables have been experimentally investigated: dynamic structure factor [1–3], electron spin resonance spectra [25], magnetic susceptibility [20], magnetocaloric effect [26], nuclear magnetic resonance relaxation rate [12], specific heat [15,16], and ultrasound velocity and attenuation [27–29].

In this work, we consider the case of a large magnetic field $B > B_c$ along the a axis, where the magnon excitations are gapped and the ground state is the fully magnetized ferromagnet. Our goal is to describe the thermal excitations above the ground state and to compare with experimental results for the specific heat [15,16]. We base our theoretical approach on a mapping of the spin-1/2 operators to hard-core bosons [30,31]. For magnetic fields $B > B_c$ and low temperatures, we then have a dilute gas of gapped hard-core bosons where the ladder approximation captures the leading order low-temperature contributions to the self-energy. Although the ladder approximation has been extensively applied to the Bose-condensed phase of dilute gases of hard-core bosons (see Ref. [18], and references therein), some subtleties related to the hard-core limit in the gapped phase have only recently been discussed by Fauseweh, Stolze, and Uhrig (FSU) [32,33]. Benchmarking the ladder approximation for an exactly solvable one-dimensional model of hard-core bosons, FSU found that the ladder approximation indeed reproduces the correct low-temperature behavior and that a self-consistent ladder approximation even extends the applicability to arbitrarily high temperatures [32]. In this work, we apply the self-consistent ladder approximation to the relevant two-dimensional model for Cs_2CuCl_4. For a realistic description of this material, we have to include additional interactions apart from the infinite on-site interaction describing the hard-core constraint. To further explore the range of validity of the self-consistent ladder approximation, we have also applied this method to the exactly solvable one-dimensional XY model; extending the analysis of FSU [32], we have examined the breakdown of the self-consistent ladder approximation in the vicinity of the quantum critical point of this model.

The rest of this work is organized as follows. In the next section, we introduce the relevant spin model for Cs_2CuCl_4 and describe the mapping of this model to an effective hard-core boson model. Then, in Sec. III, we describe our theoretical approach based on the self-consistent ladder approximation for the hard-core interaction and a self-consistent Hartree-Fock decoupling for the remaining non-hard-core interactions. In Sec. IV, we investigate the breakdown of the ladder approximation near the quantum critical point for the exactly solvable one-dimensional XY model, and in Sec. V, we present our numerical results for Cs_2CuCl_4, which we compare with experimental data for the specific heat. Finally, in Sec. VI, we summarize our main results. In three Appendices, we give additional technical details of our calculations.

*streib@itp.uni-frankfurt.de

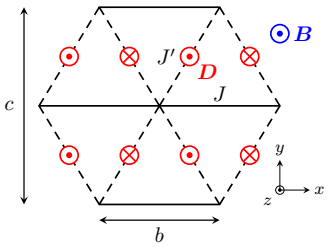

FIG. 1. (Color online) Part of the anisotropic triangular lattice formed by the spins of Cs_2CuCl_4. The stronger exchange coupling J connects nearest-neighbor spins along the crystallographic b axis, while the weaker exchange coupling J' connects nearest-neighbor spins along the diagonals. There are also weak Dzyaloshinskii-Moriya interactions $\boldsymbol{D} = \pm D\hat{\boldsymbol{z}}$ connecting neighboring spins along the diagonals where the direction of $\boldsymbol{D}$ is indicated by $\odot$ for $+\hat{\boldsymbol{z}}$ and $\otimes$ for $-\hat{\boldsymbol{z}}$. We consider only the case where the magnetic field $\boldsymbol{B} = B\hat{\boldsymbol{z}}$ is along the a axis perpendicular to the plane of the lattice.

II. HARD-CORE BOSON MODEL FOR Cs_2CuCl_4

It has been established that the magnetic behavior of Cs_2CuCl_4 can be described by the following two-dimensional antiferromagnetic spin-1/2 Heisenberg model in an external magnetic field along the crystallographic a axis [1],

$$\mathcal{H} = \frac{1}{2}\sum_{ij}[J_{ij}\boldsymbol{S}_i\cdot\boldsymbol{S}_j + \boldsymbol{D}_{ij}\cdot(\boldsymbol{S}_i\times\boldsymbol{S}_j)] - h\sum_i S_i^z, \quad (2.1)$$

where the summations run over all N lattice sites, $h = g\mu_B B$ is the Zeeman energy associated with an external magnetic field $\boldsymbol{B} = B\hat{\boldsymbol{z}}$, and $g = 2.19(1)$ is the effective g factor [1]. The spin-1/2 operators $\boldsymbol{S}_i = \boldsymbol{S}(\boldsymbol{R}_i)$ are located at the lattice sites $\boldsymbol{R}_i$ of an anisotropic triangular lattice with lattice constants b and c, as shown in Fig. 1. The exchange couplings $J_{ij} = J(\boldsymbol{R}_i - \boldsymbol{R}_j)$ connect nearest neighbors along the crystallographic b axis and along the diagonals with $J(\pm\boldsymbol{\delta}_1) = J$ and $J(\pm\boldsymbol{\delta}_2) = J(\pm\boldsymbol{\delta}_3) = J'$, where the three elementary lattice vectors are

$$\boldsymbol{\delta}_1 = b\hat{\boldsymbol{x}},\ \boldsymbol{\delta}_2 = -\frac{b}{2}\hat{\boldsymbol{x}} + \frac{c}{2}\hat{\boldsymbol{y}},\ \boldsymbol{\delta}_3 = -\frac{b}{2}\hat{\boldsymbol{x}} - \frac{c}{2}\hat{\boldsymbol{y}}. \quad (2.2)$$

Here, $\hat{\boldsymbol{x}}$, $\hat{\boldsymbol{y}}$, and $\hat{\boldsymbol{z}}$ are the unit vectors of our Cartesian coordinate system. Due to the fact that inversion symmetry is broken for Cs_2CuCl_4, there are also Dzyaloshinskii-Moriya (DM) interactions $\boldsymbol{D}_{ij} = D(\boldsymbol{R}_i - \boldsymbol{R}_j)\hat{\boldsymbol{z}}$ connecting neighboring spins along the diagonals with $D(\pm\boldsymbol{\delta}_2) = D(\pm\boldsymbol{\delta}_3) = \mp D$. The precise form of the Hamiltonian (2.1) and the values of the interaction constants have been measured by inelastic neutron scattering experiments in magnetic fields higher than the saturation field $B_c = 8.44(1)$ T. The accepted values are [1] $J = 0.374(5)$ meV $= 4.34(6)$ K, $J'/J = 0.34(3)$, and $D/J = 0.053(5)$. There is also a weak interlayer coupling $J''/J = 0.045(5)$, which we neglect because it is only important at very low temperatures $T \lesssim 0.1$ K and in the antiferromagnetically ordered phase in magnetic fields $B < B_c$, which we do not consider here. Recently, additional DM interactions, including in-plane components, have been measured via electron spin resonance experiments [25]. We neglect these additional DM interactions because they are mainly important for in-plane magnetic fields [21]. Furthermore, our theoretical approach relies on the U(1) symmetry due to the spin-rotational invariance with respect to the z axis, which would be broken by in-plane DM interactions.

In this work, we will use the hard-core boson representation of the spin-1/2 operators [30,31]. Recall that the spin-1/2 operators fulfill the commutation relations

$$[S_i^+, S_j^-] = 2\delta_{ij}S_i^z, \quad [S_i^\pm, S_j^z] = \mp\delta_{ij}S_i^\pm, \quad (2.3)$$

where $S_i^\pm = S_i^x \pm iS_i^y$ and $\boldsymbol{S}_i^2 = 3/4$. Additionally, the spin-1/2 operators obey an on-site exclusion principle [34],

$$S_i^+S_i^- + S_i^-S_i^+ = 1, \quad (S_i^+)^2 = (S_i^-)^2 = 0. \quad (2.4)$$

To realize these relations, we can express the spin operators in terms of hard-core boson creation and annihilation operators,

$$S_i^+ = b_i, \quad S_i^- = b_i^\dagger, \quad S_i^z = 1/2 - b_i^\dagger b_i, \quad (2.5)$$

where the hard-core boson operators satisfy the commutation relation

$$[b_i, b_j^\dagger] = \delta_{ij}(1 - 2b_i^\dagger b_i), \quad (2.6)$$

and the occupation number per site is restricted to $\hat{n}_i = 0$ or 1, with $\hat{n}_i = b_i^\dagger b_i$. The hard-core boson constraint and the commutation relation (2.6) can be realized by treating the hard-core bosons as canonical bosons with an infinite on-site repulsion,

$$\mathcal{H}_U = \frac{U}{2}\sum_i b_i^\dagger b_i^\dagger b_i b_i, \quad \text{with} \quad U\to\infty. \quad (2.7)$$

Note that the magnon excitations of the underlying spin system correspond to hard-core boson excitations.

Using Eq. (2.5) to express the spin operators in our Hamiltonian (2.1) in terms of hard-core bosons, we obtain the following hard-core boson Hamiltonian:

$$\mathcal{H} = \sum_{\boldsymbol{k}}\xi_{\boldsymbol{k}}b_{\boldsymbol{k}}^\dagger b_{\boldsymbol{k}} + \frac{1}{2N}\sum_{\boldsymbol{k},\boldsymbol{k}',\boldsymbol{q}}(J_{\boldsymbol{q}} + U)b_{\boldsymbol{k}+\boldsymbol{q}}^\dagger b_{\boldsymbol{k}'-\boldsymbol{q}}^\dagger b_{\boldsymbol{k}'}b_{\boldsymbol{k}} + E_0, \quad (2.8)$$

where we have Fourier transformed the hard-core boson creation and annihilation operators,

$$b_{\boldsymbol{k}} = \frac{1}{\sqrt{N}}\sum_i b_i e^{-i\boldsymbol{k}\cdot\boldsymbol{R}_i}, \quad b_{\boldsymbol{k}}^\dagger = \frac{1}{\sqrt{N}}\sum_i b_i^\dagger e^{i\boldsymbol{k}\cdot\boldsymbol{R}_i}. \quad (2.9)$$

In the following, we will neglect the unimportant constant energy term

$$E_0 = N\left(\frac{J_0}{8} - \frac{h}{2}\right). \quad (2.10)$$

The excitation energy $\xi_{\boldsymbol{k}}$ in the quadratic part of the Hamiltonian can be written as

$$\xi_{\boldsymbol{k}} = \varepsilon_{\boldsymbol{k}} - \mu, \quad (2.11)$$

where we have introduced the chemical potential

$$\mu = h_c - h \quad (2.12)$$

and the energy dispersion

$$\varepsilon_{\boldsymbol{k}} = \tfrac{1}{2}\left(J_{\boldsymbol{k}}^D - J_{\boldsymbol{Q}}^D\right). \quad (2.13)$$

Here,

$$J_{\boldsymbol{k}}^D = J_{\boldsymbol{k}} - iD_{\boldsymbol{k}}, \quad (2.14)$$

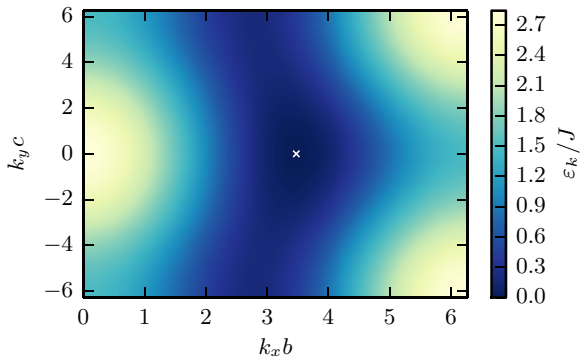

FIG. 2. (Color online) Contour plot of the energy dispersion $\varepsilon_{\boldsymbol{k}}$ defined in Eq. (2.13). The white cross marks the minimum of $\varepsilon_{\boldsymbol{k}}$ at $\boldsymbol{Q} \approx (3.474/b, 0)$.

where the Fourier transforms of the exchange and Dzyaloshinskii-Moriya interactions are

$$J_{\boldsymbol{k}} = \sum_{\boldsymbol{R}} J(\boldsymbol{R}) e^{-i\boldsymbol{k}\cdot\boldsymbol{R}} = 2J\cos(k_x b) + 4J'\cos\left(\frac{k_x b}{2}\right)\cos\left(\frac{k_y c}{2}\right), \quad (2.15)$$

$$D_{\boldsymbol{k}} = \sum_{\boldsymbol{R}} D(\boldsymbol{R}) e^{-i\boldsymbol{k}\cdot\boldsymbol{R}} = -4iD\sin\left(\frac{k_x b}{2}\right)\cos\left(\frac{k_y c}{2}\right). \quad (2.16)$$

In Eq. (2.13), $J_{\boldsymbol{Q}}^D \approx -2.325J$ is the absolute minimum of $J_{\boldsymbol{k}}^D$ at $\boldsymbol{Q} \approx (3.474/b, 0)$. Finally, the saturation field is given by

$$B_c = \frac{h_c}{g\mu_B} = \frac{1}{2g\mu_B}\left(J_0^D - J_{\boldsymbol{Q}}^D\right) \approx 8.4\ \mathrm{T}. \quad (2.17)$$

A contour plot of $\varepsilon_{\boldsymbol{k}}$ is shown in Fig. 2. In the following, we will use the direct experimental value of the saturation field $B_c = 8.44(1)$ T instead of $B_c \approx 8.4$ T because the experimental value is more accurate than a calculation via the Hamiltonian (2.8). The reason is that the interaction constants in Eq. (2.8) have some experimental uncertainty and we have also neglected the interlayer coupling J''; including J'' in the calculation would result in $B_c \approx 8.5$ T [15,17]. The value of the saturation field B_c is important because, for a given magnetic field, it determines the energy gap

$$\Delta = -\mu = h - h_c. \quad (2.18)$$

We note that a small change of B_c by 0.04 T changes the gap by about $0.014J$, which is only significant close to the quantum critical point.

III. IMPLEMENTING THE SELF-CONSISTENT LADDER APPROXIMATION

In this section, we explain our theoretical approach to the hard-core boson Hamiltonian (2.8). The central problem is how to deal with the interaction part of the Hamiltonian,

$$\mathcal{H}_{\mathrm{int}} = \frac{1}{2N}\sum_{\boldsymbol{k},\boldsymbol{k}',\boldsymbol{q}} (J_{\boldsymbol{q}} + U) b_{\boldsymbol{k}+\boldsymbol{q}}^\dagger b_{\boldsymbol{k}'-\boldsymbol{q}}^\dagger b_{\boldsymbol{k}'} b_{\boldsymbol{k}}, \quad (3.1)$$

containing the exchange interaction $J_{\boldsymbol{q}}$ and the infinite hard-core interaction $U \to \infty$. We will deal with both interactions using different methods: for the $J_{\boldsymbol{q}}$ part we use a self-consistent Hartree-Fock decoupling, while for the hard-core interaction U we use the self-consistent ladder approximation [32]. This is necessary because the $J_{\boldsymbol{q}}$ interaction cannot be easily included in the self-consistent ladder approximation, as this would not allow a direct solution for the effective interaction Γ from the Bethe-Salpeter equation which would significantly complicate matters, especially regarding the limit $U \to \infty$.

A. Hartree-Fock decoupling

We approximate the $J_{\boldsymbol{q}}$ interaction term in Eq. (3.1) using a self-consistent Hartree-Fock decoupling. Therefore we write this term in real space

$$\frac{1}{2N}\sum_{\boldsymbol{k},\boldsymbol{k}',\boldsymbol{q}} J_{\boldsymbol{q}} b_{\boldsymbol{k}+\boldsymbol{q}}^\dagger b_{\boldsymbol{k}'-\boldsymbol{q}}^\dagger b_{\boldsymbol{k}'} b_{\boldsymbol{k}} = \frac{1}{2}\sum_{i,j} J_{ij} b_i^\dagger b_i b_j^\dagger b_j, \quad (3.2)$$

and then we apply the usual Hartree-Fock decoupling

$$b_i^\dagger b_i b_j^\dagger b_j \approx n_i b_j^\dagger b_j + n_j b_i^\dagger b_i - n_i n_j + \tau_{ji} b_i^\dagger b_j + \tau_{ij} b_j^\dagger b_i - \tau_{ij}\tau_{ji}, \quad (3.3)$$

giving

$$\frac{1}{2}\sum_{i,j} J_{ij} b_i^\dagger b_i b_j^\dagger b_j \approx \sum_{i,j} J_{ij}(n_j b_i^\dagger b_i + \tau_{ji} b_i^\dagger b_j) + E_{\mathrm{MF}}, \quad (3.4)$$

where the Hartree-Fock parameters are given by

$$n_i = \langle b_i^\dagger b_i\rangle, \quad \tau_{ij} = \langle b_i^\dagger b_j\rangle, \quad (3.5)$$

and the constant energy term is

$$E_{\mathrm{MF}} = -\frac{1}{2}\sum_{i,j} J_{ij}(n_i n_j + \tau_{ij}\tau_{ji}). \quad (3.6)$$

Due to translational invariance, we have

$$n_i = n, \quad \tau_{ij} = \tau(\boldsymbol{R}_i - \boldsymbol{R}_j). \quad (3.7)$$

Because there is no inversion symmetry, $\tau(\boldsymbol{R})$ is a complex number satisfying $\tau^*(\boldsymbol{R}) = \tau(-\boldsymbol{R})$. Since the exchange coupling $J(\boldsymbol{R})$ is only nonzero for $\boldsymbol{R} = \pm\boldsymbol{\delta}_i$, there are three complex Hartree-Fock parameters related to $\tau(\boldsymbol{R})$,

$$\tau_1 = \tau(\boldsymbol{\delta}_1), \quad \tau_2 = \tau(\boldsymbol{\delta}_2), \quad \tau_3 = \tau(\boldsymbol{\delta}_3). \quad (3.8)$$

However, the Hamiltonian (2.8) is invariant under the transformation $k_y \to -k_y$ and therefore $\tau_2 = \tau_3$. Transforming Eq. (3.4) back to momentum space, we get

$$\frac{1}{2N}\sum_{\boldsymbol{k},\boldsymbol{k}',\boldsymbol{q}} J_{\boldsymbol{q}} b_{\boldsymbol{k}+\boldsymbol{q}}^\dagger b_{\boldsymbol{k}'-\boldsymbol{q}}^\dagger b_{\boldsymbol{k}'} b_{\boldsymbol{k}} \approx \sum_{\boldsymbol{k}} \left(J_{\boldsymbol{k}}^\tau + nJ_0\right) b_{\boldsymbol{k}}^\dagger b_{\boldsymbol{k}} + E_{\mathrm{MF}}, \quad (3.9)$$

where

$$J_{\boldsymbol{k}}^\tau = 2J\mathrm{Re}(\tau_1 e^{i\boldsymbol{k}\cdot\boldsymbol{\delta}_1}) + 2J'\mathrm{Re}(\tau_2 e^{i\boldsymbol{k}\cdot\boldsymbol{\delta}_2} + \tau_3 e^{i\boldsymbol{k}\cdot\boldsymbol{\delta}_3}), \quad (3.10)$$

$$E_{\mathrm{MF}} = -N\left[\frac{J_0}{2}n^2 + J|\tau_1|^2 + J'(|\tau_2|^2 + |\tau_3|^2)\right]. \quad (3.11)$$

The Hartree-Fock approximation gives a constant energy shift $E_{\rm MF}$, which depends on the magnetic field and the temperature; moreover, the Hartree-Fock approximation leads to a renormalization of single-particle excitation energies $\xi_{\boldsymbol{k}} \to \tilde{\xi}_{\boldsymbol{k}}$, where the renormalized excitation energies are

$$\tilde{\xi}_{\boldsymbol{k}} = \varepsilon_{\boldsymbol{k}} - \mu + J^{\tau}_{\boldsymbol{k}} + nJ_0. \tag{3.12}$$

The self-consistency equations for the Hartree-Fock parameters are given by

$$\tau_i = \tau(\boldsymbol{\delta}_i) = \frac{1}{N}\sum_{\boldsymbol{k}} n_{\boldsymbol{k}} e^{-i\boldsymbol{k}\cdot\boldsymbol{\delta}_i}, \tag{3.13a}$$

$$n = \frac{1}{N}\sum_{\boldsymbol{k}} n_{\boldsymbol{k}}, \tag{3.13b}$$

where the occupation number of a state with momentum $\boldsymbol{k}$ is given by

$$n_{\boldsymbol{k}} = \langle b^{\dagger}_{\boldsymbol{k}} b_{\boldsymbol{k}}\rangle. \tag{3.14}$$

If we neglect the hard-core interaction, we simply obtain the Bose-Einstein distribution,

$$n^{\rm HF}_{\boldsymbol{k}} = \frac{1}{e^{\beta\tilde{\xi}_{\boldsymbol{k}}} - 1}, \tag{3.15}$$

where $\beta = 1/T$ is the inverse temperature and the renormalized excitation energy $\tilde{\xi}_{\boldsymbol{k}}$ can be obtained in a straightforward way by solving the self-consistency equations for the Hartree-Fock parameters for $U = 0$. Neglecting the hard-core interaction is possible only for small temperatures $T \ll J$ when the bosons are so dilute that the hard-core interaction does not contribute significantly.

B. Self-consistent ladder approximation

After the Hartree-Fock decoupling of the $J_{\boldsymbol{q}}$ interaction, we obtain a Hamiltonian where the only remaining interaction is the infinite on-site repulsion,

$$\mathcal{H} = \sum_{\boldsymbol{k}} \tilde{\xi}_{\boldsymbol{k}} b^{\dagger}_{\boldsymbol{k}} b_{\boldsymbol{k}} + \frac{U}{2N}\sum_{\boldsymbol{k},\boldsymbol{k}',\boldsymbol{q}} b^{\dagger}_{\boldsymbol{k}+\boldsymbol{q}} b^{\dagger}_{\boldsymbol{k}'-\boldsymbol{q}} b_{\boldsymbol{k}'} b_{\boldsymbol{k}} + E_{\rm MF}. \tag{3.16}$$

We will deal with this hard-core interaction using the self-consistent ladder approximation developed in Ref. [32].

1. Imaginary time path integral formalism

To derive the self-consistent ladder approximation, it is convenient to formulate the problem in terms of an imaginary time path integral [35]. The Euclidean action associated with the Hamiltonian (3.16) is

$$S[\bar{b},b] = -\int_K G_0^{-1}(K)\bar{b}_K b_K + \frac{U}{2}\int_{K,K',Q} \bar{b}_{K+Q}\bar{b}_{K'-Q} b_{K'} b_K. \tag{3.17}$$

Here, we have introduced the composite index $K = (\boldsymbol{k}, i\omega_k)$ with the corresponding sum

$$\int_K = \frac{1}{\beta N}\sum_{\boldsymbol{k}}\sum_{\omega_k}, \tag{3.18}$$

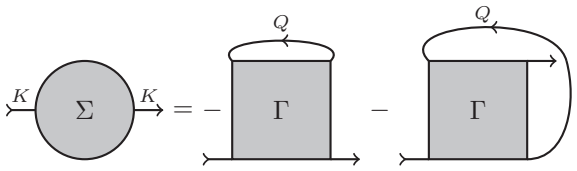

FIG. 3. Diagrammatic representation of the self-energy in terms of the effective interaction as given in Eq. (3.27).

where ω_k are bosonic Matsubara frequencies. The complex boson fields in imaginary time have been Fourier transformed to frequency space as

$$b_{\boldsymbol{k}}(\tau) = \frac{1}{\beta\sqrt{N}}\sum_{\omega_k} e^{-i\omega_k\tau} b_K, \tag{3.19a}$$

$$\bar{b}_{\boldsymbol{k}}(\tau) = \frac{1}{\beta\sqrt{N}}\sum_{\omega_k} e^{i\omega_k\tau} \bar{b}_K. \tag{3.19b}$$

The Green function $G(K)$ and the corresponding self-energy $\Sigma(K)$ are defined via the functional average

$$\langle \bar{b}_K b_K\rangle = -\beta N G(K) = -\beta N \frac{1}{G_0^{-1}(K) - \Sigma(K)}, \tag{3.20}$$

where the bare Green function $G_0(K)$ is given by

$$G_0(K) = \frac{1}{i\omega_k - \tilde{\xi}_{\boldsymbol{k}}}. \tag{3.21}$$

From this path integral formalism, a perturbative diagrammatic expansion of the one-particle irreducible self-energy $\Sigma(K)$ can be obtained in terms of the bare Green function $G_0(K)$ and the interaction U.

2. Self-consistent ladder approximation

Since we are dealing with a strictly nonperturbative problem ($U \to \infty$), it is necessary to sum over a suitable infinite set of diagrams containing infinite powers of U. Here, we approximate the self-energy by summing over all particle-particle ladder diagrams, where we express the self-energy in terms of the effective interaction Γ, as shown in Fig. 3. The effective interaction then includes the infinite series of particle-particle ladder diagrams indicated in Fig. 4. Formally, this approximation is justified for $\beta\Delta \gg 1$ because the neglected diagrams are of order $\exp(-\beta\Delta)$ smaller than the ladder diagrams. The neglected diagrams for the self-energy include at least two lines going backwards in imaginary time while the ladder diagrams only include a single line of this type; each such line gives a suppression of $\exp(-\beta\Delta)$. This can be seen

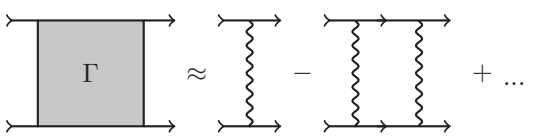

FIG. 4. Ladder approximation for the effective interaction Γ including all particle-particle ladder diagrams.

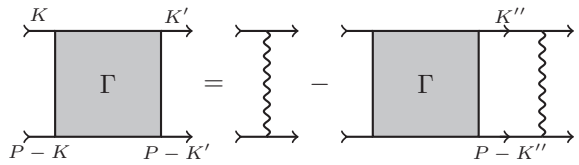

FIG. 5. Diagrammatic representation of the Bethe-Salpeter equation (3.24) for the effective interaction Γ.

by considering the bare Green function in imaginary time,

$$G_0(\boldsymbol{k},\tau) = \begin{cases} -(1+n_B(\tilde{\xi}_{\boldsymbol{k}}))e^{-\tilde{\xi}_{\boldsymbol{k}}\tau}, & \tau > 0 \\ -n_B(\tilde{\xi}_{\boldsymbol{k}})e^{-\tilde{\xi}_{\boldsymbol{k}}\tau}, & \tau < 0 \end{cases}, \tag{3.22}$$

where $n_B(x)$ denotes the Bose function,

$$n_B(x) = \frac{1}{e^{\beta x}-1}. \tag{3.23}$$

We see that $n_B(\tilde{\xi}_{\boldsymbol{k}}) \propto \exp(-\beta\Delta)$ for $\beta\Delta \gg 1$ and therefore $G_0(\boldsymbol{k},\tau) \propto \exp(-\beta\Delta)$ for $\tau < 0$.

We can go beyond the ladder approximation and include higher-order terms by using the full Green function $G(K)$ in the diagrammatic expansion instead of the bare Green function $G_0(K)$ and then finding a self-consistent solution. In this self-consistent ladder approximation, the effective interaction fulfills the Bethe-Salpeter equation shown in Fig. 5,

$$\Gamma(K',K;P) = U - U\int_{K''} \Gamma(K'',K;P)G(K'')G(P-K''). \tag{3.24}$$

Because the hard-core interaction U is a constant independent of the momentum transfer, the Bethe-Salpeter equation has the simple solution

$$\Gamma(K',K;P) = \Gamma(P) = \frac{U}{1+U\Pi(P)}, \tag{3.25}$$

where we have defined the particle-particle bubble

$$\Pi(P) = \int_Q G(Q)G(P-Q). \tag{3.26}$$

The self-energy in the self-consistent ladder approximation is given by

$$\Sigma(K) = -2\int_Q G(Q)\Gamma(Q+K)e^{i\omega_q 0^+}, \tag{3.27}$$

which is shown diagrammatically in Fig. 3. The convergence factor $e^{i\omega_q 0^+}$ implements the correct time ordering at the interaction vertex in the first order term in U where a propagator line starts and ends at the same vertex [35]. The Green function has the spectral representation

$$G(K) = \int_{-\infty}^{\infty} dx\, \frac{A(\boldsymbol{k},x)}{i\omega_k - x}, \tag{3.28}$$

where the spectral function is given by

$$\begin{aligned} A(\boldsymbol{k},\omega) &= -\frac{1}{\pi}\mathrm{Im}G(\boldsymbol{k},\omega+i0^+) \\ &= -\frac{1}{\pi}\frac{\mathrm{Im}\Sigma^R(\boldsymbol{k},\omega)}{[\omega-\tilde{\xi}_{\boldsymbol{k}}-\mathrm{Re}\Sigma^R(\boldsymbol{k},\omega)]^2+[\mathrm{Im}\Sigma^R(\boldsymbol{k},\omega)]^2}, \end{aligned} \tag{3.29}$$

and the retarded self-energy is obtained by analytic continuation to real frequencies,

$$\Sigma^R(\boldsymbol{k},\omega) = \Sigma(\boldsymbol{k},\omega+i0^+). \tag{3.30}$$

We note that the spectral function of hard-core bosons fulfills the following sum rule [32]:

$$\int_{-\infty}^{\infty} d\omega\, A(\boldsymbol{k},\omega) = \langle[b_{\boldsymbol{k}},b_{\boldsymbol{k}}^\dagger]\rangle = 1-2n, \tag{3.31}$$

with

$$n = \frac{1}{N}\sum_{\boldsymbol{k}} n_{\boldsymbol{k}} = \frac{1}{N}\sum_{\boldsymbol{k}}\int_{-\infty}^{\infty} dx\, A(\boldsymbol{k},x)n_B(x). \tag{3.32}$$

Our goal is to calculate the self-consistent solution for the spectral function $A(\boldsymbol{k},\omega)$. But before we can do this, we have to take the limit $U \to \infty$ analytically.

3. *Taking the limit $U \to \infty$*

We can write the effective interaction $\Gamma(P)$ as

$$\Gamma(P) = \frac{1}{\Pi(P)} + \delta\Gamma(P), \tag{3.33}$$

where the second term

$$\delta\Gamma(P) = -\frac{1}{\Pi(P)}\frac{1}{1+U\Pi(P)} \tag{3.34}$$

does also contribute to the $U \to \infty$ limit because the denominator of $\delta\Gamma(P)$ can vanish at high frequencies $\omega_p \sim \mathcal{O}(U)$ leading to an additional delta-function contribution, which has to be taken into account. This subtlety of the $U \to \infty$ limit has been noticed only quite recently by FSU [32]. We now follow FSU to derive the correct hard-core limit for our model. First of all, we note that $\Pi(\boldsymbol{p},\omega) \propto 1/\omega$ for $\omega \to \infty$. This allows us to introduce the spectral representation

$$\Pi(\boldsymbol{p},\omega) = \int_{-\infty}^{\infty} dx\, \frac{\rho(\boldsymbol{p},x)}{\omega-x}, \tag{3.35}$$

where

$$\begin{aligned} \rho(\boldsymbol{p},\omega) &= -\frac{1}{\pi}\mathrm{Im}\Pi(\boldsymbol{p},\omega+i0^+) \\ &= -\frac{1}{N}\sum_{\boldsymbol{q}}\int_{-\infty}^{\infty} dx\, A(\boldsymbol{q},x)A(\boldsymbol{p}-\boldsymbol{q},\omega-x) \\ &\quad\times[n_B(x)-n_B(-x)]. \end{aligned} \tag{3.36}$$

Now, we use the fact that for $\omega \to \infty$,

$$\Gamma(\boldsymbol{p},\omega) - U = \frac{-U^2\Pi(\boldsymbol{p},\omega)}{1+U\Pi(\boldsymbol{p},\omega)} \propto \frac{1}{\omega}, \tag{3.37}$$

because $\Pi(\boldsymbol{p},\omega) \propto 1/\omega$ for $\omega \to \infty$. This implies that $\Gamma(\boldsymbol{p},\omega) - U$ has the spectral representation

$$\Gamma(\boldsymbol{p},\omega) - U = \int_{-\infty}^{\infty} dx\, \frac{\bar{\rho}(\boldsymbol{p},x)}{\omega - x}, \tag{3.38}$$

where

$$\begin{aligned}\bar{\rho}(\boldsymbol{p},\omega) &= -\frac{1}{\pi}\mathrm{Im}[\Gamma(\boldsymbol{p},\omega + i0^+)] \\ &= f(\boldsymbol{p},\omega) - \frac{1}{\pi}\mathrm{Im}[\delta\Gamma(\boldsymbol{p},\omega + i0^+)],\end{aligned} \tag{3.39}$$

with

$$f(\boldsymbol{p},\omega) = \frac{-\rho(\boldsymbol{p},\omega)}{\left[\mathcal{P}\int_{-\infty}^{\infty} dx\, \frac{\rho(\boldsymbol{p},x)}{\omega - x}\right]^2 + [\pi\rho(\boldsymbol{p},\omega)]^2}. \tag{3.40}$$

Here, $\mathcal{P}$ denotes the Cauchy principal value which arises from the identity $1/(\omega + i0^+) = \mathcal{P}(1/\omega) - i\pi\delta(\omega)$. For the contribution of $\delta\Gamma$ to $\bar{\rho}(\boldsymbol{p},\omega)$, we recall that the denominator of $\delta\Gamma(\boldsymbol{p},\omega)$ can vanish when $\omega \sim \mathcal{O}(U)$ and only in that case there can be a contribution from $\delta\Gamma$. Therefore we expand $\Pi(\boldsymbol{p},\omega)$ for large frequencies $\omega \sim \mathcal{O}(U)$ (we take U to be very large but finite),

$$\Pi(\boldsymbol{p},\omega) \approx \frac{\rho_0(\boldsymbol{p})}{\omega} + \frac{\rho_1(\boldsymbol{p})}{\omega^2} + \mathcal{O}\left(\frac{1}{\omega^3}\right), \tag{3.41}$$

where

$$\rho_0(\boldsymbol{p}) = \int_{-\infty}^{\infty} dx \rho(\boldsymbol{p},x), \tag{3.42a}$$

$$\rho_1(\boldsymbol{p}) = \int_{-\infty}^{\infty} dx\, x\rho(\boldsymbol{p},x). \tag{3.42b}$$

We find

$$\begin{aligned}\delta\Gamma(P) \approx &-\frac{1}{\frac{\rho_0(\boldsymbol{p})}{\omega} + \frac{\rho_1(\boldsymbol{p})}{\omega^2} + \mathcal{O}\left(\frac{1}{\omega^3}\right)} \\ &\times \frac{1}{1 + U\frac{\rho_0(\boldsymbol{p})}{\omega} + U\frac{\rho_1(\boldsymbol{p})}{\omega^2} + \mathcal{O}\left(\frac{U}{\omega^3}\right)},\end{aligned} \tag{3.43}$$

where the terms $\mathcal{O}(1/\omega^3)$ and $\mathcal{O}(U/\omega^3)$ vanish at the pole $\omega \sim \mathcal{O}(U)$ in the limit $U \to \infty$, justifying the expansion to order $1/\omega^2$. Therefore we have

$$\delta\Gamma(P) \approx -\frac{1}{\frac{\rho_0(\boldsymbol{p})}{\omega} + \frac{\rho_1(\boldsymbol{p})}{\omega^2}} \frac{\omega^2}{(\omega - \omega_1(\boldsymbol{p}))(\omega - \omega_2(\boldsymbol{p}))}, \tag{3.44}$$

where the poles are given by

$$\begin{aligned}\omega_1(\boldsymbol{p}) &= -\frac{U\rho_0(\boldsymbol{p})}{2} - \sqrt{\frac{U^2\rho_0^2(\boldsymbol{p})^2}{4} - U\rho_1(\boldsymbol{p})} \\ &\sim -U\rho_0(\boldsymbol{p}), \quad U \to \infty,\end{aligned} \tag{3.45a}$$

$$\begin{aligned}\omega_2(\boldsymbol{p}) &= -\frac{U\rho_0(\boldsymbol{p})}{2} + \sqrt{\frac{U^2\rho_0^2(\boldsymbol{p})}{4} - U\rho_1(\boldsymbol{p})} \\ &\sim -\frac{\rho_1(\boldsymbol{p})}{\rho_0(\boldsymbol{p})}, \quad U \to \infty.\end{aligned} \tag{3.45b}$$

Only the pole at $\omega_1 \sim \mathcal{O}(U)$ is relevant for the analytic continuation in Eq. (3.39) because the other pole at $\omega_2 \sim \mathcal{O}(U^0)$ is spurious, since we have expanded for large frequencies $\omega \sim \mathcal{O}(U)$. In total, we get

$$\bar{\rho}(\boldsymbol{p},\omega) = f(\boldsymbol{p},\omega) - \frac{1}{\frac{\rho_0(\boldsymbol{p})}{\omega} + \frac{\rho_1(\boldsymbol{p})}{\omega^2}} \frac{\omega^2}{\omega - \omega_2(\boldsymbol{p})}\delta(\omega - \omega_1(\boldsymbol{p})). \tag{3.46}$$

We can now use the spectral representation (3.38) in Eq. (3.27) and take the limit $U \to \infty$ to get the following expression for the self-energy:

$$\begin{aligned}\Sigma(K) = &-\frac{2}{N}\sum_{\boldsymbol{q}}\int_{-\infty}^{\infty} dx \int_{-\infty}^{\infty} dx' A(\boldsymbol{q},x') f(\boldsymbol{q}+\boldsymbol{k},x) \\ &\times \frac{n_B(x) - n_B(x')}{i\omega_k + x' - x} + \frac{2}{N}\sum_{\boldsymbol{q}}\int_{-\infty}^{\infty} dx\, A(\boldsymbol{q},x) n_B(x) \\ &\times\left[\frac{x + i\omega_k}{\rho_0(\boldsymbol{q}+\boldsymbol{k})} - \frac{\rho_1(\boldsymbol{q}+\boldsymbol{k})}{\rho_0^2(\boldsymbol{q}+\boldsymbol{k})}\right].\end{aligned} \tag{3.47}$$

By analytic continuation to real frequencies, we obtain the real and imaginary parts of the retarded self-energy:

$$\begin{aligned}\mathrm{Re}\Sigma^R(\boldsymbol{k},\omega) = &\frac{2}{N}\sum_{\boldsymbol{q}}\int_{-\infty}^{\infty} dx\, A(\boldsymbol{q},x) n_B(x) \\ &\times\left[\frac{x+\omega}{\rho_0(\boldsymbol{q}+\boldsymbol{k})} - \frac{\rho_1(\boldsymbol{q}+\boldsymbol{k})}{\rho_0^2(\boldsymbol{q}+\boldsymbol{k})}\right] \\ &+ \mathcal{P}\int_{-\infty}^{\infty} dx\, \frac{\rho_\Sigma(\boldsymbol{k},x)}{\omega - x},\end{aligned} \tag{3.48a}$$

$$\mathrm{Im}\Sigma^R(\boldsymbol{k},\omega) = -\pi\rho_\Sigma(\boldsymbol{k},\omega), \tag{3.48b}$$

where

$$\begin{aligned}\rho_\Sigma(\boldsymbol{k},\omega) = &\frac{2}{N}\sum_{\boldsymbol{q}}\int_{-\infty}^{\infty} dx\, A(\boldsymbol{q},x) f(\boldsymbol{q}+\boldsymbol{k},x+\omega) \\ &\times[n_B(x) - n_B(x+\omega)].\end{aligned} \tag{3.48c}$$

To summarize, we have obtained the self-energy in the limit $U \to \infty$, which we can calculate starting from an initial spectral function. Via Eq. (3.29) we can then calculate the next iteration of the spectral function allowing us to find a self-consistent solution for the spectral function. After each iteration, the Hartree-Fock parameters n, τ_1, τ_2, and τ_3 have to be updated via the self-consistency equations (3.13a) and (3.13b) using

$$n_{\boldsymbol{k}} = \langle b_{\boldsymbol{k}}^\dagger b_{\boldsymbol{k}}\rangle = \int_{-\infty}^{\infty} dx\, A(\boldsymbol{k},x) n_B(x). \tag{3.49}$$

IV. NUMERICAL RESULTS FOR THE ONE-DIMENSIONAL XY MODEL

Before applying the above approach to the hard-core boson model for Cs_2CuCl_4, it is instructive to test its validity for the exactly solvable one-dimensional spin-1/2 XY model in a magnetic field. Although a similar model has been already studied in detail in Ref. [32], the breakdown of the self-consistent ladder approximation in the vicinity of the quantum critical point has not been investigated.

The XY model in one dimension is given by

$$\mathcal{H}_{1D} = J\sum_i \left(S_i^x S_{i+1}^x + S_i^y S_{i+1}^y\right) - h\sum_i S_i^z, \tag{4.1}$$

which can again be mapped to hard-core bosons (neglecting constant terms)

$$\mathcal{H}_{1D} = \sum_k \xi_k b_k^\dagger b_k + \frac{U}{2N}\sum_{k,k',q} b_{k+q}^\dagger b_{k'-q}^\dagger b_{k'} b_k, \tag{4.2}$$

with excitation energy

$$\xi_k = J[\cos(k_x b) + 1] - \mu, \tag{4.3}$$

where $\mu = h_c - h = -\Delta$ and $h_c = J$. An exact solution can be found by mapping the hard-core bosons to fermions via the Jordan-Wigner transformation,

$$b_j = e^{-i\pi\sum_{l<j} c_l^\dagger c_l} c_j, \quad b_j^\dagger = c_j^\dagger e^{i\pi\sum_{l<j} c_l^\dagger c_l}, \tag{4.4}$$

resulting in the quadratic Hamiltonian

$$\mathcal{H}_{1D} = \sum_k \xi_k c_k^\dagger c_k, \tag{4.5}$$

where the operators $c_k^\dagger$ and c_k are fermionic creation and annihilation operators. The hard-core boson density is therefore exactly given by

$$n = \frac{1}{N}\sum_k \frac{1}{e^{\beta\xi_k}+1}, \tag{4.6}$$

which can be compared to the approximate solution from the self-consistent ladder approximation for the hard-core boson model. We note that for low temperatures at $\mu = 0$, the exact density (4.6) has the following asymptotic behavior:

$$n \sim \frac{\sqrt{2T/J}}{\pi}\int_0^\infty dx\, \frac{1}{e^{x^2}+1} \approx 0.241\sqrt{T/J}, \tag{4.7}$$

in agreement with the expected behavior of one-dimensional bosons at the quantum critical point [36].

In Fig. 6, we compare the approximate result for the boson density n obtained within the self-consistent ladder approximation with the exact solution. The relative error $\delta n/n$ of the approximate result is shown in Fig. 7 where we define

$$\delta n/n = \frac{n_{\text{ladder}} - n_{\text{exact}}}{n_{\text{exact}}}. \tag{4.8}$$

Here, n_{ladder} is the result from the self-consistent ladder approximation and n_{exact} is the exact result. For a finite gap, we see that the error vanishes for low and high temperatures with a maximum error at $T \approx \Delta$, while the error becomes smaller for larger energy gaps. For $\Delta = 0$, the error keeps increasing for smaller temperatures, getting closer to the quantum critical point at $T = 0$, but decreases for higher temperatures. We conclude that the self-consistent ladder approximation gives good results over the whole temperature range for finite energy gaps $\Delta \gtrsim 0.1J$.

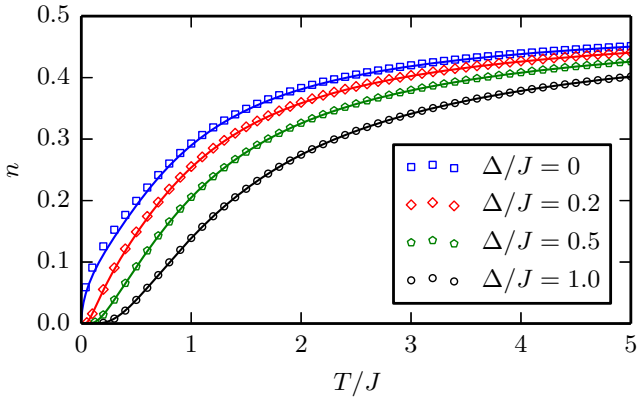

FIG. 6. (Color online) Comparison of the results for the boson density n obtained from the self-consistent ladder approximation (symbols) with the exact result (solid lines) at different energy gaps Δ for the one-dimensional XY model.

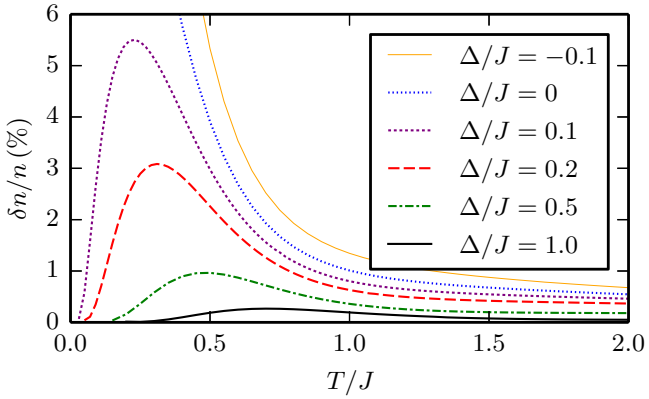

FIG. 7. (Color online) Relative error $\delta n/n$ of the boson density [see Eq. (4.8)] in the self-consistent ladder approximation for the one-dimensional XY model as a function of temperature at different energy gaps Δ.

V. NUMERICAL RESULTS FOR Cs_2CuCl_4

In this section, we apply our hard-core boson approach described in Sec. III to the relevant model for Cs_2CuCl_4 given in Sec. II. From the numerical solution of the self-consistent ladder approximation we calculate the spectral function of the hard-core bosons at finite temperatures for different magnetic fields in the regime $B > B_c$ where the energy gap $\Delta > 0$ is finite. Given the spectral function, we can calculate the magnetization, the internal energy, and the transverse part of the spin dynamic structure factor. From the magnetization and internal energy, we obtain the magnetic susceptibility and the specific heat by numerical differentiation. Finally, we compare our results with experimental data for the specific heat [15,16]. Technical details of the numerical solution of the self-consistent ladder approximation can be found in Appendices A and B.

1. Spectral function

Due to the finite energy gap $\Delta > 0$, at zero temperature the spectral function is exactly given by the noninteracting spectral function,

$$A(\boldsymbol{k},\omega) = A_0(\boldsymbol{k},\omega) = \delta(\omega - \xi_{\boldsymbol{k}}). \tag{5.1}$$

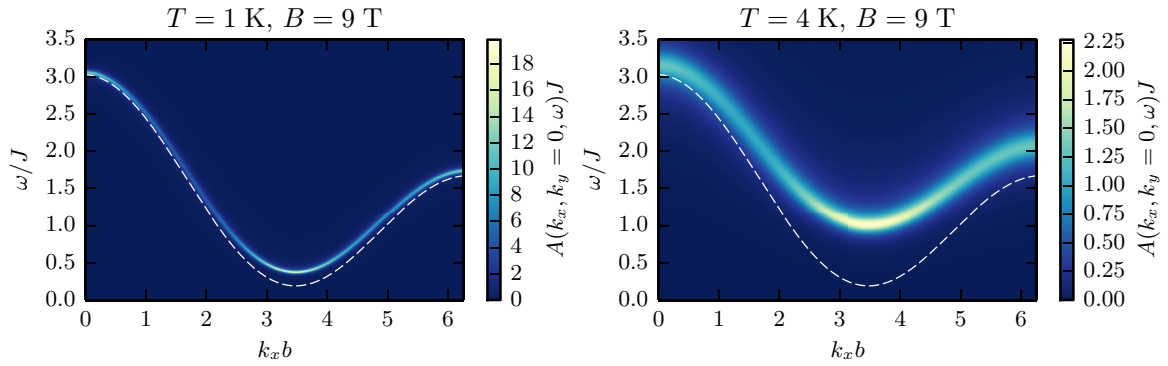

FIG. 8. (Color online) Contour plots of the spectral function $A(\boldsymbol{k},\omega)$ of the hard-core bosons at $k_y = 0$ for temperatures of 1 and 4 K in a magnetic field $B = 9$ T corresponding to an energy gap $\Delta = 0.19J$. The white dashed line is the bare excitation energy $\xi_{\boldsymbol{k}}$ given by Eq. (2.11).

At finite temperatures, interactions will lead to a renormalization of the excitation energy $\xi_{\boldsymbol{k}}$ and a broadening of the delta peaks. Since we are treating the $J_{\boldsymbol{q}}$ interaction term on a Hartree-Fock level, this alone would only renormalize the excitation energy by $\xi_{\boldsymbol{k}} \to \tilde{\xi}_{\boldsymbol{k}}$ resulting in

$$A(\boldsymbol{k},\omega) = \delta(\omega - \tilde{\xi}_{\boldsymbol{k}}). \tag{5.2}$$

Taking in addition the hard-core interaction via the self-consistent ladder approximation into account will lead to a broadening of the spectral function with rising temperature, as shown in Fig. 8. Besides the broadening, we notice that the bandwidth shrinks with rising temperature and the minimum of the spectral function gets shifted to higher energies increasing the effective energy gap from its bare value Δ at $T = 0$. In Fig. 9, we contrast the behavior of the spectral function at $\boldsymbol{k} = 0$ and at the minimum of the dispersion $\boldsymbol{k} = \boldsymbol{Q}$. While at $\boldsymbol{k} = 0$ the position of the peak only moves to slightly higher energies, at the minimum of the dispersion the peak gets considerably shifted to higher energies. Due to the finite frequency resolution in our numerical calculation (see Appendix A), we cannot reach arbitrarily low temperatures and are restricted to temperatures $T \gtrsim 0.2\Delta$ where the spectral function is not too narrow to be resolved. However, in the temperature range $T \lesssim 0.2\Delta$, the hard-core interaction can be neglected and we can then just use the self-consistent Hartree-Fock decoupling without hard-core interaction, as we will show further below.

The spectral function can be related to the in-plane components of the spin dynamic structure factor. The spin dynamic structure factor is defined by

$$S^{\alpha\beta}(\boldsymbol{k},\omega) = \int_{-\infty}^{\infty} \frac{dt}{2\pi} e^{i\omega t} \left\langle S^{\alpha}_{-\boldsymbol{k}}(t) S^{\beta}_{\boldsymbol{k}}(0) \right\rangle, \tag{5.3}$$

where $\alpha,\beta = x,y,z$ and the Fourier transforms of the spin operators are defined via

$$S^{\alpha}_{\boldsymbol{k}} = \frac{1}{\sqrt{N}} \sum_i e^{-i\boldsymbol{k}\cdot\boldsymbol{R}_i} S^{\alpha}_i. \tag{5.4}$$

The in-plane components of the spin dynamic structure factor are given by

$$\begin{aligned} S^{xx}(\boldsymbol{k},\omega) &= S^{yy}(\boldsymbol{k},\omega) \\ &= \frac{1}{4} \frac{1}{1 - e^{-\beta\omega}} (A(\boldsymbol{k},\omega) + A(-\boldsymbol{k},\omega)), \end{aligned} \tag{5.5a}$$

$$\begin{aligned} S^{xy}(\boldsymbol{k},\omega) &= -S^{yx}(\boldsymbol{k},\omega) \\ &= \frac{1}{4} \frac{1}{1 - e^{-\beta\omega}} (A(\boldsymbol{k},\omega) - A(-\boldsymbol{k},\omega)), \end{aligned} \tag{5.5b}$$

where $S^{xy}(\boldsymbol{k},\omega)$ and $S^{yx}(\boldsymbol{k},\omega)$ do not vanish due to the broken inversion symmetry. The U(1) symmetry due to the spin-rotational invariance with respect to the z axis requires that

$$S^{xz}(\boldsymbol{k},\omega) = S^{zx}(\boldsymbol{k},\omega) = S^{yz}(\boldsymbol{k},\omega) = S^{zy}(\boldsymbol{k},\omega) = 0. \tag{5.6}$$

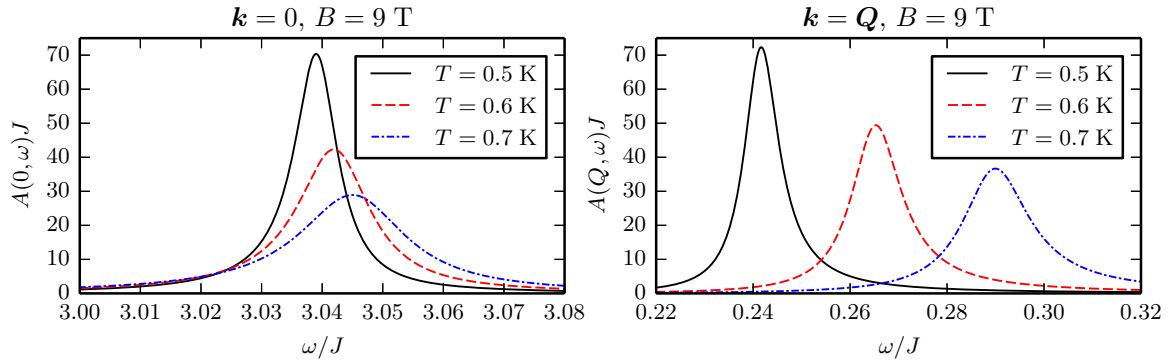

FIG. 9. (Color online) Spectral function $A(\boldsymbol{k},\omega)$ at $\boldsymbol{k} = 0$ and at $\boldsymbol{k} = \boldsymbol{Q}$ (at the minimum of the dispersion) in a magnetic field $B = 9$ T corresponding to an energy gap $\Delta \approx 0.19J$.

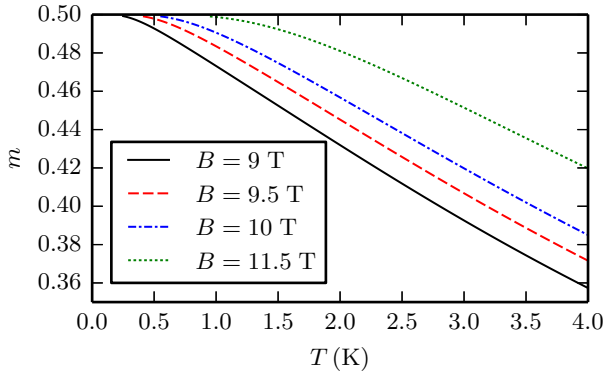

FIG. 10. (Color online) Numerical results for the magnetic moment m at different magnetic fields between 9 and 11.5 T.

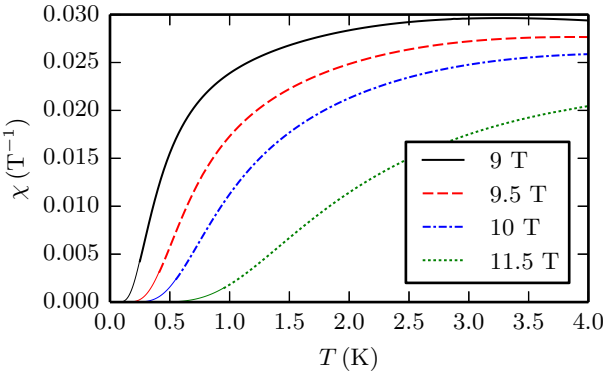

FIG. 11. (Color online) Numerical results for the magnetic susceptibility χ at different magnetic fields between 9 and 11.5 T. The thin solid lines are low-temperature results from the Hartree-Fock approximation without hard-core interaction, which allows us to get results in the low-temperature regime where the self-consistent ladder approximation cannot be used due to the limited frequency resolution.

The S^{zz} component of the spin dynamic structure factor cannot be simply expressed in terms of the spectral function because it is a two-particle Green function in terms of the hard-core boson operators:

$$S^{zz}(\boldsymbol{k},\omega) = \frac{1}{N}\sum_{\boldsymbol{q},\boldsymbol{q}'}\int_{-\infty}^{\infty}\frac{dt}{2\pi}e^{i\omega t}\langle b^{\dagger}_{\boldsymbol{q}}(t)b_{\boldsymbol{q}-\boldsymbol{k}}(t)b^{\dagger}_{\boldsymbol{q}'}(0)b_{\boldsymbol{q}'+\boldsymbol{k}}(0)\rangle. \tag{5.7}$$

2. *Magnetic moment and magnetic susceptibility*

The magnetic moment per site is given by

$$m = \langle S^z_i\rangle = \tfrac{1}{2} - n, \tag{5.8}$$

where n is the boson density per site which can be expressed in terms of the spectral function,

$$n = \frac{1}{N}\sum_{\boldsymbol{k}} n_{\boldsymbol{k}}, \tag{5.9}$$

with

$$n_{\boldsymbol{k}} = \langle b^{\dagger}_{\boldsymbol{k}} b_{\boldsymbol{k}}\rangle = \int_{-\infty}^{\infty} dx\, A(\boldsymbol{k},x) n_B(x). \tag{5.10}$$

We define the magnetic susceptibility χ via

$$\chi = \frac{dm}{dB}. \tag{5.11}$$

In the limit $T \to 0$, the boson density vanishes and the asymptotic low-temperature behavior of the susceptibility is therefore the one of free bosons because all interaction are frozen out,

$$\chi \propto T^{\frac{d-2}{2}} e^{-\Delta/T}, \tag{5.12}$$

where d is the dimensionality ($d = 2$ in our case) and Δ the energy gap.

The numerical results for magnetic moment and magnetic susceptibility for different magnetic fields above the saturation field are shown in Figs. 10 and 11, respectively. In Fig. 12, we compare our numerical results from the self-consistent ladder approximation with the low-temperature Hartree-Fock approximation without hard-core interaction and with a simple spin mean-field theory, which we describe in Appendix C. We see that for low temperatures $T \ll J$ the Hartree-Fock and the ladder approximation give essentially the same results. This allows us to use the Hartree-Fock approximation in the low-temperature regime where the self-consistent ladder approximation is difficult to implement due to the limited frequency resolution. At higher temperatures, the hard-core interaction becomes important and the high-temperature behavior is approximately captured by the spin mean-field theory.

3. *Internal energy and specific heat*

The internal energy is given by

$$E = \langle \mathcal{H}\rangle = \sum_{\boldsymbol{k}} \tilde{\xi}_{\boldsymbol{k}} n_{\boldsymbol{k}} + E_{\mathrm{MF}}, \tag{5.13}$$

where the infinite on-site interaction does not contribute because its expectation value is zero if the hard-core constraint is fulfilled. The specific heat at constant volume is obtained by

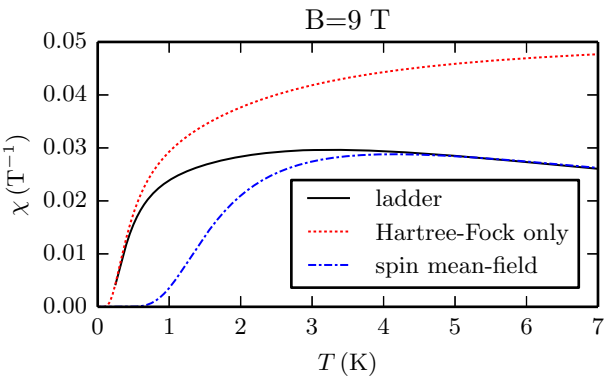

FIG. 12. (Color online) Comparison of the results for the magnetic susceptibility χ from the self-consistent ladder approximation, Hartree-Fock approximation without hard-core interaction, and spin mean-field theory for a magnetic field $B = 9$ T corresponding to an energy gap $\Delta \approx 0.19J$.

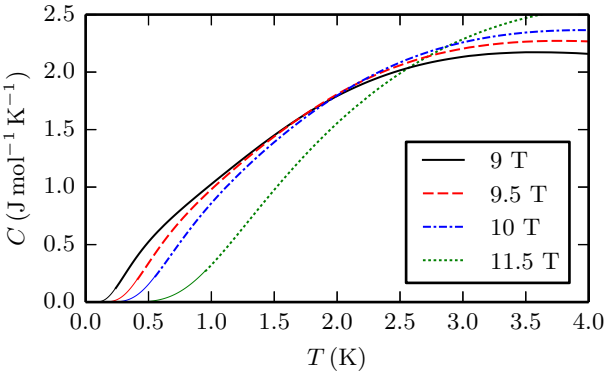

FIG. 13. (Color online) Numerical results for the specific heat C at different magnetic fields between 9 and 11.5 T. The thin solid lines are low-temperature results from the Hartree-Fock approximation without hard-core interaction, which allows us to get results in the low-temperature regime where the self-consistent ladder approximation cannot be used due to the limited frequency resolution.

taking the temperature derivative of the internal energy,

$$C = \frac{dE}{dT}. \tag{5.14}$$

We note that E_{MF} depends on temperature and has to be taken into account for calculating the specific heat. The asymptotic low-temperature behavior of the specific heat is given by

$$C \propto T^{\frac{d-4}{2}} e^{-\Delta/T}. \tag{5.15}$$

The numerical results for the specific heat at different magnetic fields above the saturation field are shown in Fig. 13. In Fig. 14, we again compare our numerical results from the self-consistent ladder approximation with the low-temperature Hartree-Fock approximation without hard-core interaction and with a simple spin mean-field theory described in Appendix C. The magnetic contribution to the specific heat of Cs_2CuCl_4 has been measured experimentally [15,16]. The more recent data published in Ref. [16] differ slightly from Ref. [15] for $B = 11.5$ T and are in better agreement with the expected size of the energy gap at that field strength. Therefore, in Fig. 15, we

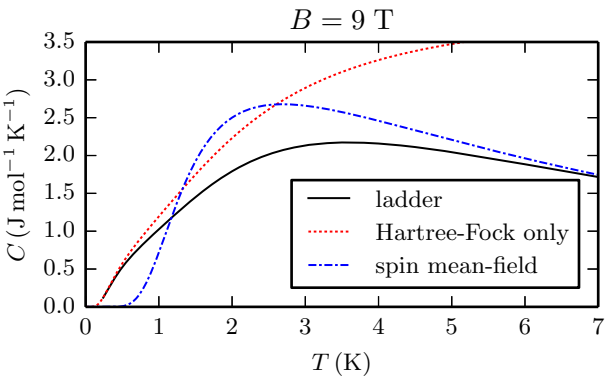

FIG. 14. (Color online) Comparison of the results for the specific heat C from the self-consistent ladder approximation, Hartree-Fock approximation without hard-core interaction, and spin mean-field theory for a magnetic field $B = 9$ T corresponding to an energy gap $\Delta \approx 0.19J$.

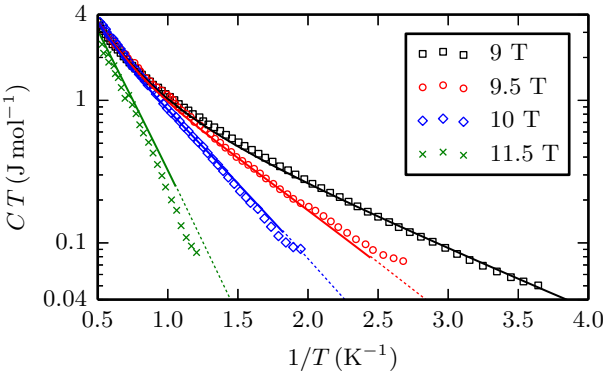

FIG. 15. (Color online) Comparison of our numerical results for the specific heat (solid lines) with experimental data from Ref. [16] (symbols) for different magnetic fields between 9 and 11.5 T. The dashed lines are low-temperature results from the Hartree-Fock approximation without hard-core interaction, which allows us to get results in the low-temperature regime where the self-consistent ladder approximation cannot be used due to the limited frequency resolution.

compare our results with the experimental data from Ref. [16], where we find that our theory captures the experimentally observed behavior both qualitatively and quantitatively. At low temperatures, the slope in the logarithmic plot of CT versus $1/T$ in Fig. 15 is given by $-\Delta$, which follows directly from Eq. (5.15).

VI. SUMMARY AND CONCLUSIONS

We have mapped the spin-1/2 Heisenberg model describing Cs_2CuCl_4 to a model of hard-core bosons where the hard-core constraint has been taken into account by an infinite on-site repulsion. Since we have only considered magnetic fields $B > B_c$ (along the a axis perpendicular to the lattice plane), we had to deal with gapped hard-core bosons. Due to the energy gap, the hard-core interaction can be taken into account using the self-consistent ladder approximation [32] and the remaining interactions can be treated within the self-consistent Hartree-Fock approximation. Before applying this method to Cs_2CuCl_4, we have investigated for the exactly solvable one-dimensional XY model how the ladder approximation breaks down in the vicinity of the critical field B_c, finding that the ladder approximation for finite energy gaps Δ works well both at low and high temperatures and the deviations, maximal at $T \approx \Delta$, decrease with rising energy gap Δ. We have then calculated the spectral function of the hard-core bosons for Cs_2CuCl_4 from which we have obtained the magnetic susceptibility and the specific heat. The calculated specific heat is in good agreement with the available experimental data. We conclude that the self-consistent ladder approximation in combination with a self-consistent Hartree-Fock decoupling of the non-hard-core interactions gives an accurate description of the physical properties of gapped hard-core bosons in two dimensions at finite temperatures. An extension to three dimensions is straightforward and would only increase the numerical effort due to an increasing number of lattice sites. Our methods can also be directly applied to the material class $Cs_2Cu(Cl_{4-x}Br_x)$, where chlorine is partially substituted by

bromine which changes the strength of the exchange couplings and the ratio J'/J [37–39]. While in our work we started from a spin-1/2 model which we mapped to hard-core bosons, our theoretical approach is applicable whenever the elementary excitations can be described by gapped hard-core bosons; some examples are discussed in Ref. [32]. In the case of $S > 1/2$, a mapping to hard-core bosons is not known, but mapping the spins to canonical bosons is possible by using, for example, the Holstein-Primakoff transformation [40], where the constraint on the boson occupation number per site, $\hat{n}_i \leqslant 2S$, is difficult to take into account analytically. Therefore spin-wave theories based on such a mapping to canonical bosons are only valid for low boson densities at low temperatures, where the constraint is not important and the usual expansion in $\hat{n}_i/S$ is justified.

ACKNOWLEDGMENTS

We thank Michael Lang, Lars Postulka, and Bernd Wolf for useful discussions. Financial support by the DFG via SFB/TRR49 is gratefully acknowledged.

APPENDIX A: NUMERICAL DETAILS

In this Appendix, we give more details on the numerical solution of the self-consistency equations for the spectral function $A(\boldsymbol{k},\omega)$. To find a self-consistent solution for $A(\boldsymbol{k},\omega)$, we have to start from an initial spectral function $A_{\text{init}}(\boldsymbol{k},\omega)$. If we would just have the standard non-self-consistent ladder approximation, we would replace $A(\boldsymbol{k},\omega)$ by the noninteracting spectral function $A_0(\boldsymbol{k},\omega)$ and then directly calculate the spectral function $A(\boldsymbol{k},\omega)$. It is therefore sensible to use the noninteracting spectral function as the initial spectral function, which is given by

$$A_0(\boldsymbol{k},\omega) = -\frac{1}{\pi}\text{Im}G_0(\boldsymbol{k},\omega + i0^+) = \delta(\omega - \xi_{\boldsymbol{k}}). \tag{A1}$$

We note here that at $T = 0$ the spectral function is not affected by interactions, $A(\boldsymbol{k},\omega) = A_0(\boldsymbol{k},\omega)$, because the ground state is the vacuum without any bosons due to the energy gap. For the numerical calculation, we replace the delta function by a box function of finite width η (e.g., $\eta = 0.1J$) centered at $\omega = \xi_{\boldsymbol{k}}$. This is fine as long as $\xi_{\boldsymbol{k}} > 0$ which is the case for magnetic fields $B > B_c$. For $\xi_{\boldsymbol{k}} \leqslant 0$, we have to take the sign of the spectral function into account [35],

$$\text{sgn}(A(\boldsymbol{k},\omega)) = \text{sgn}\,\omega. \tag{A2}$$

Therefore a positive delta peak is not permitted for negative frequencies and the noninteracting spectral function cannot be used for values of $\boldsymbol{k}$ with $\xi_{\boldsymbol{k}} \leqslant 0$. In our calculations, we instead place a step function at a small positive frequency when $\xi_{\boldsymbol{k}} \leqslant 0$. This allows us to find a self-consistent solution even for $B \leqslant B_c$.

Having chosen an initial spectral function, the next step is to calculate $\rho(\boldsymbol{p},\omega)$ via Eq. (3.36), which is a multidimensional convolution that can be calculated with the fast Fourier transform method, e.g., using the FFTW library [41]. Then $f(\boldsymbol{p},\omega)$ can be obtained from Eq. (3.40), where the principal value integral can also be evaluated as a convolution [42]. Next, the calculation of $\rho_\Sigma(\boldsymbol{k},\omega)$ via Eq. (3.48c) and $\text{Re}\Sigma^R(\boldsymbol{k},\omega)$ via Eq. (3.48a) also involves convolutions. While the values of $\boldsymbol{k}$ are naturally discretized for a finite lattice, as discussed in Appendix B, the real frequencies ω have to be artificially discretized, leading to a limited frequency resolution, and a frequency cutoff has to be introduced (e.g., $|\omega| < 20J$). When using the fast Fourier transform method to evaluate the convolutions, this treats the functions as periodic both in momentum and frequency space, leading to a wrap-around effect in the frequency dependence of the calculated functions. This wrap-around error can be dealt with by setting the spectral function $A(\boldsymbol{k},\omega)$ to zero for frequencies larger than a certain cutoff (e.g., for $|\omega| > 10J$). In our calculations, we typically used lattice sizes up to 4096 sites and up to 131 072 frequency points.

To achieve convergence, a simple mixing update procedure has to be used, where the updated spectral function and Hartree-Fock parameters are set to be a mixture of the previous iteration and the new values from the self-consistency equations. In our case, a mixing of 50% worked well. We note that in the case without the self-consistent Hartree-Fock decoupling (e.g., for an XY model), mixing is not necessary to achieve convergence. The converged numerical result should (up to a small numerical error) fulfill the sum rule [32]

$$\int_{-\infty}^{\infty} d\omega\, A(\boldsymbol{k},\omega) = 1 - 2n. \tag{A3}$$

APPENDIX B: BRILLOUIN ZONE DISCRETIZATION

The use of fast Fourier transform methods is based on the periodicity of the transformed functions. Therefore the Brillouin zone should not be arbitrarily discretized because that would in most cases destroy the periodicity. Still, there is an infinite number of possible parametrizations of the Brillouin zone. In our work, we have used two parametrizations, which we will present here. The first parametrization starts from the lattice basis

$$\boldsymbol{a}_1 = b\hat{\boldsymbol{x}}, \quad \boldsymbol{a}_2 = -\frac{b}{2}\hat{\boldsymbol{x}} + \frac{c}{2}\hat{\boldsymbol{y}}, \tag{B1}$$

with the corresponding reciprocal basis

$$\boldsymbol{b}_1 = \frac{2\pi}{b}\hat{\boldsymbol{x}} + \frac{2\pi}{c}\hat{\boldsymbol{y}}, \quad \boldsymbol{b}_2 = \frac{4\pi}{c}\hat{\boldsymbol{y}}. \tag{B2}$$

The lattice momentum vectors can then be expanded in terms of the reciprocal basis,

$$\boldsymbol{k} = k_1\boldsymbol{b}_1 + k_2\boldsymbol{b}_2, \tag{B3}$$

where the periodic boundary conditions dictate that

$$k_1 = \frac{l_1}{N_1}, \quad l_1 \in \{0,\ldots,N_1 - 1\}, \tag{B4a}$$

$$k_2 = \frac{l_2}{N_2}, \quad l_2 \in \{0,\ldots,N_2 - 1\}. \tag{B4b}$$

The total number of lattice sites is $N = N_1N_2$. To obtain a uniform mesh [43], we have to choose

$$N_2 = 2N_1. \tag{B5}$$

The second (primed) parametrization starts from the lattice basis

$$\boldsymbol{a}_1' = \frac{b}{2}\hat{\boldsymbol{x}} - \frac{c}{2}\hat{\boldsymbol{y}}, \quad \boldsymbol{a}_2' = \frac{b}{2}\hat{\boldsymbol{x}} + \frac{c}{2}\hat{\boldsymbol{y}}, \tag{B6}$$

with the corresponding reciprocal basis

$$\boldsymbol{b}_1' = \frac{2\pi}{b}\hat{\boldsymbol{x}} - \frac{2\pi}{c}\hat{\boldsymbol{y}}, \quad \boldsymbol{b}_2' = \frac{2\pi}{b}\hat{\boldsymbol{x}} + \frac{2\pi}{c}\hat{\boldsymbol{y}}. \tag{B7}$$

The lattice momentum vectors can again be expanded in terms of the reciprocal basis,

$$\boldsymbol{k} = k_1'\boldsymbol{b}_1' + k_2'\boldsymbol{b}_2', \tag{B8}$$

where the periodic boundary conditions dictate that

$$k_1' = \frac{l_1'}{N_1'}, \quad l_1' \in \{0, \ldots, N_1' - 1\}, \tag{B9a}$$

$$k_2' = \frac{l_2'}{N_2'}, \quad l_2' \in \{0, \ldots, N_2' - 1\}. \tag{B9b}$$

The total number of lattice sites is $N = N_1'N_2'$. To obtain a uniform mesh [43], we have to choose

$$N_2' = N_1'. \tag{B10}$$

APPENDIX C: SPIN MEAN-FIELD APPROXIMATION

We expect that at high temperatures $T \gg J$, the spins decouple and it is sufficient to describe the spin-spin interactions on a mean-field level where the effects of the interactions are approximated by an effective magnetic field. To derive this mean-field description, we start from the Hamiltonian (2.1),

$$\mathcal{H} = \frac{1}{2}\sum_{ij}[J_{ij}\boldsymbol{S}_i \cdot \boldsymbol{S}_j + \boldsymbol{D}_{ij} \cdot (\boldsymbol{S}_i \times \boldsymbol{S}_j)] - h\sum_i S_i^z. \tag{C1}$$

First, we note that only the z component of the expectation values of the spin operators does not vanish,

$$\langle \boldsymbol{S}_i \rangle = m\hat{\boldsymbol{z}}, \quad m = \langle S_i^z \rangle. \tag{C2}$$

Expanding up to linear order in fluctuations from this expectation value, we find

$$\mathcal{H} \approx -NJ_0\frac{m^2}{2} - h_{\text{eff}}\sum_i S_i^z, \tag{C3}$$

where the effective magnetic field is given by

$$h_{\text{eff}} = h - J_0 m, \tag{C4}$$

with

$$J_0 = 2J + 4J'. \tag{C5}$$

The magnetic moment m is obtained by solving the self-consistency equation

$$m = \frac{1}{2}\tanh\left(\frac{\beta}{2}h_{\text{eff}}\right), \tag{C6}$$

and the energy in this mean-field approximation is a simple function of magnetic field and magnetic moment,

$$E = N\left(\tfrac{1}{2}J_0 m^2 - mh\right). \tag{C7}$$

[1] R. Coldea, D. A. Tennant, K. Habicht, P. Smeibidl, C. Wolters, and Z. Tylczynski, Phys. Rev. Lett. **88**, 137203 (2002).
[2] R. Coldea, D. A. Tennant, A. M. Tsvelik, and Z. Tylczynski, Phys. Rev. Lett. **86**, 1335 (2001).
[3] R. Coldea, D. A. Tennant, and Z. Tylczynski, Phys. Rev. B **68**, 134424 (2003).
[4] S. Yunoki and S. Sorella, Phys. Rev. B **74**, 014408 (2006).
[5] M. Q. Weng, D. N. Sheng, Z. Y. Weng, and R. J. Bursill, Phys. Rev. B **74**, 012407 (2006).
[6] Y. Hayashi and M. Ogata, J. Phys. Soc. Jpn. **76**, 053705 (2007).
[7] M. Kohno, O. A. Starykh, and L. Balents, Nat. Phys. **3**, 790 (2007).
[8] M. Kohno, Phys. Rev. Lett. **103**, 197203 (2009).
[9] D. Heidarian, S. Sorella, and F. Becca, Phys. Rev. B **80**, 012404 (2009).
[10] L. Balents, Nature (London) **464**, 199 (2010).
[11] T. Tay and O. I. Motrunich, Phys. Rev. B **81**, 165116 (2010).
[12] M.-A. Vachon, G. Koutroulakis, V. F. Mitrović, O. Ma, J. B. Marston, A. P. Reyes, P. Kuhns, R. Coldea, and Z. Tylczynski, New J. Phys. **13**, 093029 (2011).
[13] T. Herfurth, S. Streib, and P. Kopietz, Phys. Rev. B **88**, 174404 (2013).
[14] L. F. Tocchio, C. Gros, R. Valentí, and F. Becca, Phys. Rev. B **89**, 235107 (2014).
[15] T. Radu, H. Wilhelm, V. Yushankhai, D. Kovrizhin, R. Coldea, Z. Tylczynski, T. Lühmann, and F. Steglich, Phys. Rev. Lett. **95**, 127202 (2005).
[16] T. Radu, Y. Tokiwa, R. Coldea, P. Gegenwart, Z. Tylczynski, and F. Steglich, Sci. Technol. Adv. Mater. **8**, 406 (2007).
[17] D. L. Kovrizhin, V. Yushankhai, and L. Siurakshina, Phys. Rev. B **74**, 134417 (2006).
[18] V. Zapf, M. Jaime, and C. D. Batista, Rev. Mod. Phys. **86**, 563 (2014).
[19] M. Y. Veillette, J. T. Chalker, and R. Coldea, Phys. Rev. B **71**, 214426 (2005).
[20] Y. Tokiwa, T. Radu, R. Coldea, H. Wilhelm, Z. Tylczynski, and F. Steglich, Phys. Rev. B **73**, 134414 (2006).
[21] O. A. Starykh, H. Katsura, and L. Balents, Phys. Rev. B **82**, 014421 (2010).
[22] C. Griset, S. Head, J. Alicea, and O. A. Starykh, Phys. Rev. B **84**, 245108 (2011).
[23] R. Chen, H. Ju, H.-C. Jiang, O. A. Starykh, and L. Balents, Phys. Rev. B **87**, 165123 (2013).
[24] O. A. Starykh, Rep. Prog. Phys. **78**, 052502 (2015).
[25] S. A. Zvyagin, D. Kamenskyi, M. Ozerov, J. Wosnitza, M. Ikeda, T. Fujita, M. Hagiwara, A. I. Smirnov, T. A. Soldatov, A. Y. Shapiro, J. Krzystek, R. Hu, H. Ryu, C. Petrovic, and M. E. Zhitomirsky, Phys. Rev. Lett. **112**, 077206 (2014).
[26] M. Lang, B. Wolf, A. Honecker, L. Balents, U. Tutsch, P. T. Cong, G. Hofmann, N. Krüger, F. Ritter, W. Assmus, and A. Prokofiev, Phys. Status Solidi B **250**, 457 (2013).
[27] A. Sytcheva, O. Chiatti, J. Wosnitza, S. Zherlitsyn, A. A. Zvyagin, R. Coldea, and Z. Tylczynski, Phys. Rev. B **80**, 224414 (2009).

[28] A. Kreisel, P. Kopietz, P. T. Cong, B. Wolf, and M. Lang, Phys. Rev. B **84**, 024414 (2011).
[29] S. Streib, P. Kopietz, P. T. Cong, B. Wolf, M. Lang, N. van Well, F. Ritter, and W. Assmus, Phys. Rev. B **91**, 041108(R) (2015).
[30] T. Matsubara and H. Matsuda, Prog. Theor. Phys. **16**, 569 (1956).
[31] E. G. Batyev and L. S. Braginskii, Sov. Phys. JETP **60**, 781 (1984).
[32] B. Fauseweh, J. Stolze, and G. S. Uhrig, Phys. Rev. B **90**, 024428 (2014).
[33] B. Fauseweh and G. S. Uhrig, arXiv:1507.03793.
[34] Y. R. Wang and M. J. Rice, Phys. Rev. B **45**, 5045 (1992).
[35] J. W. Negele and H. Orland, *Quantum Many-Particle Systems* (Addison-Wesley, Redwood City, CA, 1988).
[36] S. Sachdev, T. Senthil, and R. Shankar, Phys. Rev. B **50**, 258 (1994).
[37] N. Krüger, S. Belz, F. Schossau, A. A. Haghighirad, P. T. Cong, B. Wolf, S. Gottlieb-Schoenmeyer, F. Ritter, and W. Assmus, Cryst. Growth Des. **10**, 4456 (2010).
[38] P. T. Cong, B. Wolf, M. de Souza, N. Krüger, A. A. Haghighirad, S. Gottlieb-Schoenmeyer, F. Ritter, W. Assmus, I. Opahle, K. Foyevtsova, H. O. Jeschke, R. Valentí, L. Wiehl, and M. Lang, Phys. Rev. B **83**, 064425 (2011).
[39] K. Foyevtsova, I. Opahle, Y.-Z. Zhang, H. O. Jeschke, and R. Valentí, Phys. Rev. B **83**, 125126 (2011).
[40] T. Holstein and H. Primakoff, Phys. Rev. **58**, 1098 (1940).
[41] M. Frigo and S. Johnson, Proc. IEEE **93**, 216 (2005).
[42] H.-P. Liu and D. D. Kosloff, Geophys. J. Royal Astr. Soc. **67**, 791 (1981).
[43] J. Moreno and J. M. Soler, Phys. Rev. B **45**, 13891 (1992).